

Variable spreading layer in 4U 1608–52 during thermonuclear X-ray bursts in the soft state

J. J. E. Kajava,^{1,2} K. I. I. Koljonen,^{1,3} J. Nättilä,^{2,4} V. Suleimanov^{5,6} and J. Poutanen^{2,4,7}

¹*Finnish Centre for Astronomy with ESO (FINCA), University of Turku, Väisäläntie 20, FI-21500 Piikkiö, Finland*

²*Tuorla Observatory, Department of Physics and Astronomy, University of Turku, Väisäläntie 20, FI-21500 Piikkiö, Finland*

³*Aalto University, Metsähovi Radio Observatory, Metsähovintie 114, FI-02540 Kylmälä, Finland*

⁴*Nordita, KTH Royal Institute of Technology and Stockholm University, Roslagstullsbacken 23, SE-10691 Stockholm, Sweden*

⁵*Institut für Astronomie und Astrophysik, Kepler Center for Astro and Particle Physics, Universität Tübingen, Sand 1, D-72076 Tübingen, Germany*

⁶*Kazan (Volga region) Federal University, Kremlevskaya str. 18, Kazan 420008, Russia*

⁷*Kavli Institute for Theoretical Physics, University of California, Santa Barbara, CA 93106, USA*

Accepted 2017 July 28. Received 2017 July 28; in original form 2017 May 10

ABSTRACT

Thermonuclear (type-I) X-ray bursts, observed from neutron star (NS) low-mass X-ray binaries (LMXB), provide constraints on NS masses and radii and consequently the equation of state of NS cores. In such analyses various assumptions are made without knowing if they are justified. We have analyzed X-ray burst spectra from the LMXB 4U 1608–52, with the aim of studying how the different persistent emission components react to the bursts. During some bursts in the soft spectral state we find that there are two variable components; one corresponding to the burst blackbody component and another optically thick Comptonized component. We interpret the latter as the spreading layer between the NS surface and the accretion disc, which is not present during the hard state bursts. We propose that the spectral changes during the soft state bursts are driven by the spreading layer that could cover almost the entire NS in the brightest phases due to the enhanced radiation pressure support provided by the burst, and that the layer subsequently returns to its original state during the burst decay. When deriving the NS mass and radius using the soft state bursts two assumptions are therefore not met: the NS is not entirely visible and the burst emission is reprocessed in the spreading layer, causing distortions of the emitted spectrum. For these reasons the NS mass and radius constraints using the soft state bursts are different compared to the ones derived using the hard state bursts.

Key words: X-rays: binaries – stars: neutron – X-rays: bursts

1 INTRODUCTION

Thermonuclear (type I) X-ray bursts are triggered by unstable hydrogen and helium burning in a neutron star (NS) envelope (see Lewin et al. 1993, for review). The fuel is provided by a low-mass binary companion, from which gas is accumulated onto the NS through an accretion disc. The thermonuclear explosions can occasionally be so intense that the Eddington limit is exceeded for a few seconds, which causes the entire NS photosphere to expand and subsequently contract back towards the NS surface (Swank et al. 1977; Hoffman et al. 1980; Paczyński 1983). These photospheric radius expansion (PRE) bursts form a very interesting subset of X-ray bursts, because they allow the determination of the NS radius R_{NS} and mass M_{NS} simultaneously (see Nättilä et al.

2016; Özel et al. 2016; Suleimanov et al. 2017, for most recent measurements). Consequently, PRE-bursts can be used to place constraints on the NS equation of state models that describe the properties of the ultra dense matter in NS cores (Lattimer 2012).

In low-mass X-ray binaries (LMXB) the accretion onto the NS may proceed in two distinct ways, which manifest themselves as spectral states. Broadly speaking, at the lowest fluxes LMXBs are in the so called hard spectral state (or island state), whereas at higher fluxes LMXBs are in the soft spectral state (see the review by Done et al. 2007 for NS-LMXB spectral state classifications). In many respects the spectral hysteresis patterns are similar to the ones seen in the black hole binaries (see, e.g., Muñoz-Darias et al. 2014), but the NS surface plays a crucial role in creating differ-

ences. In the hard state, when the accretion disc near the NS is thought to puff up to an optically thin and geometrically thick flow, the hot electrons, protons and ions deposit most of their energy at the upper atmosphere layers (Bildsten et al. 1992). This heated NS atmosphere then acts as an extra source of soft seed photons for Comptonization in the hot flow, leading to cooler equilibrium electron temperatures and softer X-ray spectra than in black hole binaries (e.g. Done et al. 2007; Burke et al. 2017). Only in the soft state the hot inner flow may collapse into a thin disc that extends all the way down to the NS surface. In this case an optically thick boundary/spreading layer forms in between the disc and the NS surface (Inogamov & Sunyaev 1999, 2010; Suleimanov & Poutanen 2006), which emits slightly hotter quasi-thermal emission than the accretion disc with roughly the same luminosity (Gilfanov et al. 2003; Revnivtsev & Gilfanov 2006; Revnivtsev et al. 2013).

In order to measure R_{NS} and M_{NS} using X-ray bursting NS-LMXBs, several of the following simplifying assumptions are commonly made:

- (i) the NS is entirely visible during the X-ray burst, rather than being partially obscured by the accretion disc and the spreading layer (Lapidus & Sunyaev 1985);
- (ii) the burst emission is isotropic, although the reprocessing in the disc can cause the emission to be anisotropic (Lapidus & Sunyaev 1985);
- (iii) X-ray burst spectra are well described by a blackbody, but clear deviations are known to occur (e.g., Worpel et al. 2015);
- (iv) the emission region radius can be obtained from the observed blackbody radii using colour corrections from the NS atmosphere models (e.g. Suleimanov et al. 2012), but the majority of bursts are inconsistent with these model predictions, particularly those occurring in the soft spectral state (Kajava et al. 2014);
- (v) the NS photospheric composition remains constant during the bursts, while there is evidence that the nuclear burning ashes produced in the bursts may reach the photosphere, changing the spectral hardening (i.e. colour correction factors, Nättilä et al. 2015) and imprinting photo-ionization edges to the spectra (in’t Zand & Weinberg 2010; Kajava et al. 2017a), and
- (vi) the persistent (accretion) emission stays constant during the burst, even though recently several findings suggest that the persistent emission components are disturbed by the X-ray bursts (e.g., Worpel et al. 2015).

It is possible that all, some or even none of these assumptions are actually reasonable, and it remains contentious to what extent they can affect the NS mass and radius constraints.

In this paper, we study the above effects in the X-ray bursts observed from the transient NS-LMXB 4U 1608–52. In Section 2, we describe how we have reduced and analyzed the data used in this study. In Section 3, we mainly focus on the finding that one of the spectral components detected in the persistent emission is also strongly variable during the soft state X-ray bursts. This component is consistent with the optically thick spreading layer, which is not found in the hard state bursts. The behavior in the soft state bursts of 4U 1608–52 is similar to the spectral evolution seen during the superburst of 4U 1636–536 (Koljonen et al. 2016), whereas the X-ray bursts taking place during

the hard spectral state are much better described by the blackbody model. In Section 4, we discuss the main implication of our results, namely, that the spreading layer may occasionally cover almost the entire NS. This effect is not accounted for in studies that use soft state X-ray bursts for NS mass and radius determination (e.g. Güver et al. 2010; Özel et al. 2016), and likely causes the differences in NS mass and radius constraints obtained from the hard state bursts (Poutanen et al. 2014).

2 RXTE/PCA OBSERVATIONS OF 4U 1608–52

We have identified and extracted time resolved spectra of all X-ray bursts from 4U 1608–52 that have been observed with the Proportional Counter Array (PCA) instrument (Jahoda et al. 2006) onboard the *Ross X-ray Timing Explorer* (RXTE) spacecraft. We have also extracted X-ray spectra of the accretion (persistent) spectrum outside the burst intervals, in order to characterize the spectral states of this LMXB. These data have already been analyzed and presented in Poutanen et al. (2014) and Kajava et al. (2014) and, therefore, we only repeat here the most relevant points.

The PCA burst data were extracted using 0.25–4 s time intervals depending on the instrument count rate. We employed two different methods to model these spectra. The first method used the standard approach – used also in Poutanen et al. (2014) and Kajava et al. (2014) – where the accretion spectra prior to X-ray bursts were subtracted as the background. In the second method we extracted a 160 s segment prior to the burst from the “standard 2” PCA data mode (using only the events recorded by the top layer of PCU2), modeled it as described below, and then fixed some model parameters to the best-fitting values when modeling the burst spectra. We used shorter exposure times for bursts that took place less than 160 s from the start of a stable spacecraft pointing.

The spectra were deadtime corrected, and they were fitted in the 3–20 keV spectral range in XSPEC v.12.8 (Arnaud 1996). In all cases the interstellar absorption was modeled using the TBABS model (Wilms et al. 2000), with the hydrogen column density fixed to $N_{\text{H}} = 0.89 \times 10^{22} \text{ cm}^{-2}$ (Keek et al. 2008). The burst emission was described with the blackbody model, yielding a blackbody temperature T_{bb} and normalization $K_{\text{bb}} = (R_{\text{bb}}/d_{10})^2$, where R_{bb} is the blackbody radius in units of km and d_{10} is the distance to the source in units of 10 kpc. The persistent emission was modeled using three components: the accretion disc (DISKBB), the spreading layer (COMPTT) and a weak iron emission line (GAUSS) that was present in most of the persistent emission data sets. The fluxes were obtained using the CFLUX convolution model and the model errors were derived with the ERROR command at 1σ confidence level.

3 RESULTS

3.1 NMF spectral decomposition of bursts

After re-inspecting the blackbody fitting results for the soft state PRE bursts presented in Poutanen et al. (2014) and Kajava et al. (2014), we identified four PRE bursts that have large reduced χ^2 values (up to ~ 4), i.e. they showed

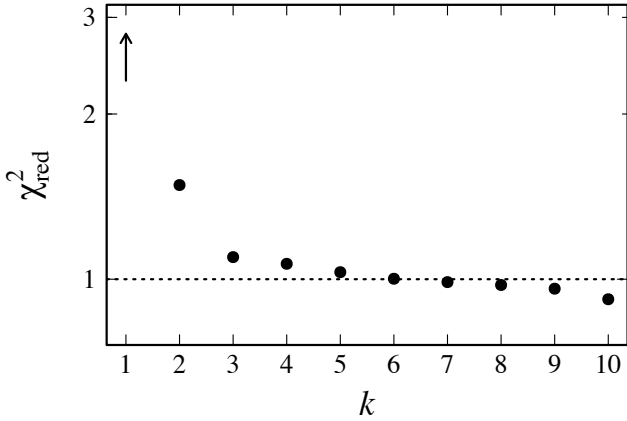


Figure 1. The χ^2 -diagram used for the determination of the degree of factorization for NMF analysis using data from the four soft-state PRE-bursts of 4U 1608–52 (not subtracting the background) that have the most non-Planckian spectra (see Fig. 5). The diagram shows a kink at $k=3$ after which further increase of the degree of factorization reduces the χ^2_{red} -value only insignificantly. Similarly to the 4U 1636–536 superburst (Koljonen et al. 2016), three components are enough to explain the spectral variability during the soft state PRE bursts of 4U 1608–52. The χ^2_{red} -value for the one-component factorization is ≈ 28 .

clear deviations from the Planckian spectra. These are the bursts observed in 1998 March 27 (OBSID 30062-01-01-00), 2002 September 09 (OBSID 70059-01-21-00), 2002 September 12 (OBSID 70059-03-01-000) and 2011 June 13 (OBSID 96423-01-11-01). Following Koljonen et al. (2016), we used the non-parametric non-negative matrix factorization (NMF) spectral decomposition technique to determine the possible causes behind the poor fits. In NMF, the observations X_{ji} , where i is the observation number and j is the spectral channel number, are approximated as a linear decomposition of a small number (k) of NMF (spectral) components W_{jk} that vary in normalization according to their signal S_{ki} , i.e. $X_{ji} \approx \sum_k W_{jk} S_{ki}$. W and S are found iteratively by minimizing a cost function (generalized Kullback-Leibler divergence) and requiring that W and S retain only positive values. We refer the reader to Koljonen (2015), and references therein for a more detailed discussion about the NMF.

We first determined the degree of NMF factorization using the χ^2 -diagram method (Koljonen 2015; Koljonen et al. 2016), shown in Fig. 1. We find that, similarly to the 4U 1636–536 superburst (Koljonen et al. 2016), three NMF components are needed to describe the spectral variability during the bursts.

In Fig. 2 we show the spectra (W_{jk}) of the three NMF components from multiple runs. The solutions are not unique, which results in a spread of the spectral shape of the individual NMF components. Nevertheless, the resulting NMF components are distinguishable from each other. As in the NMF analysis of the 4U 1636–536 superburst in Koljonen et al. (2016), we interpret the NMF components to arise from a spreading layer varying in normalization ($k=1$) and a variable burst emission varying in normalization and temperature ($k=2,3$). Note that due to the non-linear effect of the varying blackbody temperature the burst emis-

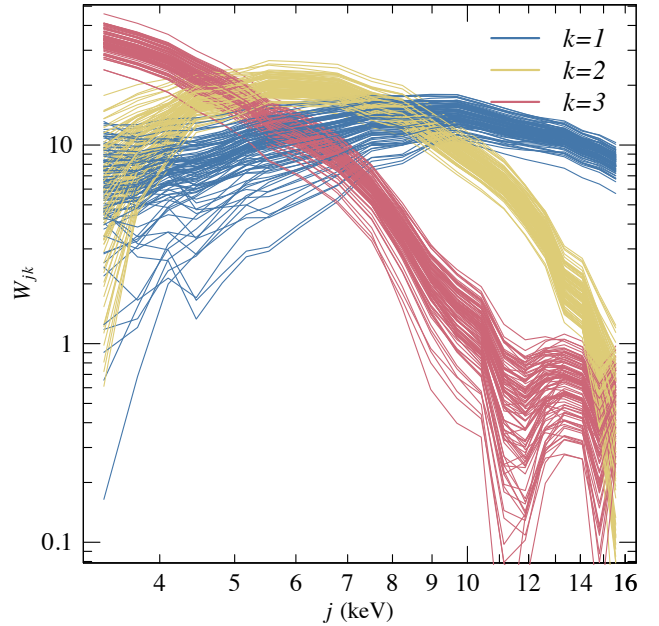


Figure 2. A sample of spectra (W_{jk}) from multiple NMF runs on the four non-Planckian soft state PRE bursts of 4U 1608–52 (background was not subtracted). The spectra have the same overall shape as in the 4U 1636–536 superburst data; the $k=1$ thus corresponds to the constant temperature spreading layer component and the $k=2$ and $k=3$ components together can be interpreted as the variable temperature burst emission.

sion gets approximated with two NMF components. We find that the averaged NMF component $k=1$ from multiple runs is well described with a COMPTT model, with the seed photon temperature, electron temperature and optical depth of $T_{\text{seed}} \approx 1.4$ keV, $T_e \approx 3$ keV and $\tau \approx 20$, respectively. T_{seed} and τ are tightly correlated parameters in the fitting, so one of them needs to be fixed to derive constrained confidence intervals. For example, if τ is fixed to 12, then $T_{\text{seed}} \approx 1.5$ keV (with the 90 per cent confidence region being between 1.2 and 1.9 keV) and $T_e \approx 3.3 \pm 0.1$ keV (at 90 per cent confidence). We note, however, that the fits have $\chi^2 = 2.7$ for 18 d.o.f., that results from the $k=1$ component having very low flux at energies below ~ 6 keV. This causes the lowest flux bins to have very high uncertainties, and thus the low energy slope is not well defined. Therefore, a blackbody model with $T_{\text{bb}} \approx 3.1$ keV can be fitted to the $k=1$ data with similar fit quality. These parameters are very similar to the COMPTT model parameters of the variable spreading layer component observed during the persistent emission of NS-LMXBs (including 4U 1608–52, see Revnivtsev & Gilfanov 2006), who obtained $T_{\text{seed}} \approx 1.5$ keV, $T_e \approx 3.3$ keV and $\tau \approx 5$.

In Fig. 3 we show the time evolution of the NMF signals (S_{ki}). The first component, $k=1$, corresponding to the spreading layer, shows the highest signal strength during 3–7 s from the burst onset, and then decays much faster than the other two components. On the other hand, both $k=2$ and $k=3$ components show very similar time evolution, which is indicative that they are generated by one spectral component changing both in flux and shape. Their sum, shown with green lines in the bottom right panel of Fig. 3, is the

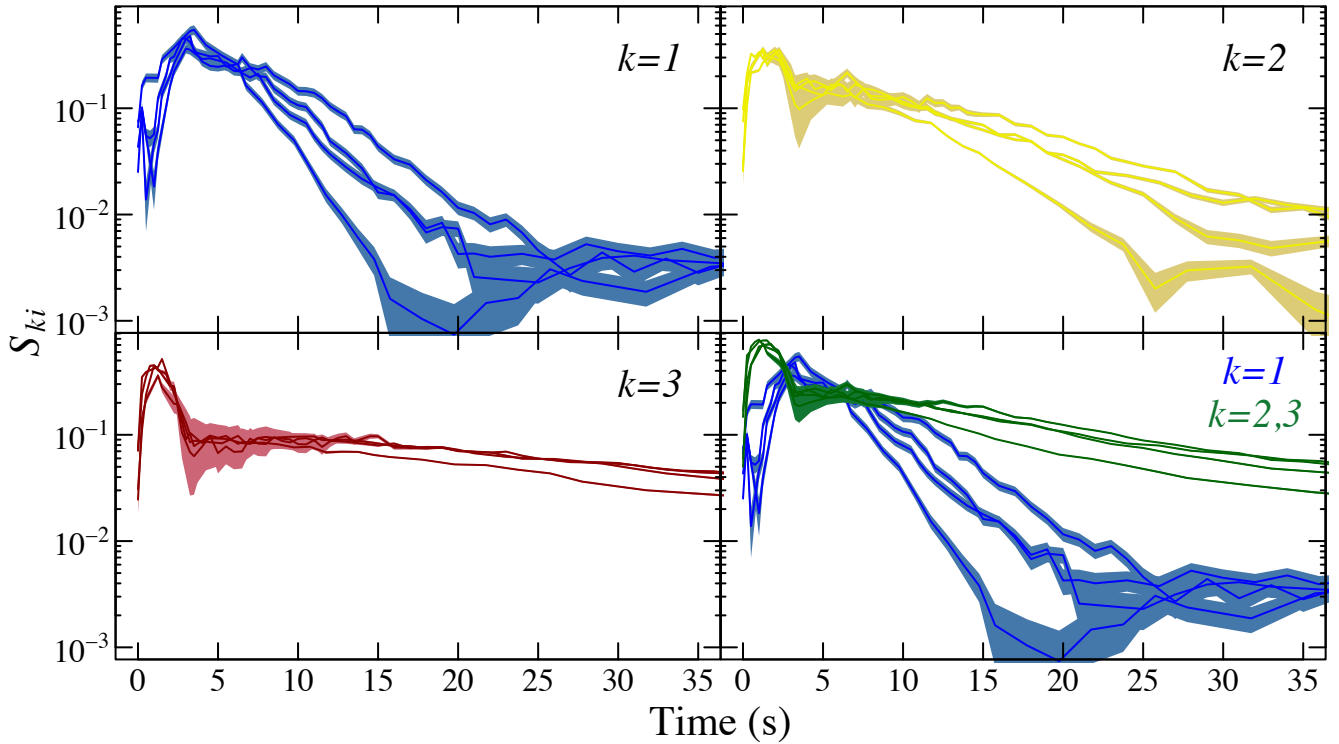


Figure 3. Time evolution of the NMF signals, S_{ki} , for the four non-Planckian bursts. The $k=1$ component (which we interpret as the spreading layer) is the dominant component between 3–7 s from the burst onset. In the PRE-phases 0–3 s and the burst tails >7 s the sum of the $k=2,3$ components (green lines; which we interpret as the variable temperature blackbody component) dominates. The leveling off of the $k=1$ signal at ~15–25 s corresponds to the time where the spreading layer emission reaches the level observed prior to the burst onset (see text and Fig. 5).

dominant component in the burst tail, after ~7 s from the burst onsets.

3.2 Modeling of the persistent emission

We started the spectral analysis by modeling the persistent emission prior to the burst onsets. The model we employed consists of four components, TBABS \times (DISKBB + COMPTT + GAUSS), which were fitted in the 3–20 keV band. The best fitting parameters for the persistent emission for this model are shown for the eight soft state PRE bursts in Table 1, with the four highly non-Planckian bursts highlighted in bold face. The seed photon temperature was fixed to $T_{\text{seed}} = 1.5$ keV, the electron temperature to 3.3 keV and the iron line energy and width to 6.4 and 0.5 keV, respectively. The X-ray fluxes were computed in the 0.01–100 keV band using the CFLUX convolution model.

The model fits the data rather well, with the best fitting COMPTT optical depths consistent with each other among the persistent spectra with a mean of $\tau \approx 3.59$, although for observations of IDs 30062-01-01-00 and 70059-03-01-000 the model is not statistically acceptable. The DISKBB normalizations, on the other hand, allows us to estimate the inner disc radius. We obtain a mean value of $R_{\text{in}} \approx 10.7$ km (minimum and maximum values being $R_{\text{in,min}} \approx 8.0$ and $R_{\text{in,max}} \approx 13.5$ km) using equation (1) of Gierliński & Done (2002), and assuming the distance of $d = 3.6$ kpc, the colour-correction

factor of $f_c = 1.8$, inclination of 60° and the correction term for the inner disc boundary condition of $\eta = 2.7$. Thus, the disc component is consistent of being extended to the NS surface. We also see that the COMPTT component carries approximately 35–55 per cent of the estimated bolometric flux. Importantly, the COMPTT parameters are in agreement with the NMF decomposition results of the bursts as well as with the frequency-resolved spectroscopic measurements of the persistent emission made by Revnivtsev & Gilfanov (2006).

3.3 Burst modeling

In addition to the standard blackbody fits where the persistent emission is removed as a background, we also modeled all the burst spectra with a two-component model using the aforementioned two methods (see Section 2). In the first method we removed the background as before, but described the X-ray burst emission with the blackbody model and used the Comptonization model COMPTT as an additional component. In the second method we did not remove the persistent emission as a background, but instead we fixed the DISKBB and GAUSS components to the values obtained prior to the bursts, and allowed only the COMPTT component to vary.

After series of tests, we decided to fix the COMPTT model parameters to the average best fitting values of the variable spreading layer component observed during the persistent

Table 1. Best-fitting parameters from modeling the persistent spectra prior to the onset of the soft state bursts using TBABS × (DISKBB + GAUSS + COMPTT) model. The first column is the observation ID, where the observations with highly non-Planckian X-ray burst spectra shown in Fig. 5 are highlighted with bold face fonts. Note that the electron temperature and several model parameters were fixed during the fitting (see text). The Gaussian line equivalent widths were approximately 50 eV.

OBS ID	T_{dbb} (keV)	K_{dbb}	F_{dbb} (10^{-9} cgs)	K_{Fe} $\times 10^{-3}$	τ	K_{ctt}	F_{ctt} (10^{-9} cgs)	$\chi^2/\text{d.o.f.}$
30062-01-01-00	$0.881^{+0.013}_{-0.013}$	280^{+20}_{-20}	$3.67^{+0.03}_{-0.02}$	$2.1^{+0.5}_{-0.5}$	$3.32^{+0.06}_{-0.06}$	$0.115^{+0.002}_{-0.002}$	$2.213^{+0.02}_{-0.013}$	61.6/42
70058-01-39-00	$0.95^{+0.02}_{-0.02}$	170^{+20}_{-20}	$2.99^{+0.06}_{-0.06}$	$3.3^{+0.6}_{-0.6}$	$4.07^{+0.06}_{-0.06}$	$0.179^{+0.002}_{-0.002}$	$3.69^{+0.02}_{-0.02}$	42.6/35
70059-01-20-00	$0.99^{+0.04}_{-0.03}$	300^{+50}_{-50}	$6.22^{+0.2}_{-0.12}$	< 1.8	$3.75^{+0.2}_{-0.13}$	$0.174^{+0.006}_{-0.007}$	$3.47^{+0.03}_{-0.05}$	38.0/35
70059-01-21-00	$1.09^{+0.02}_{-0.02}$	230^{+20}_{-20}	$7.01^{+0.06}_{-0.05}$	$3.4^{+0.8}_{-0.8}$	$3.73^{+0.06}_{-0.06}$	$0.229^{+0.004}_{-0.004}$	$4.57^{+0.03}_{-0.02}$	42.9/35
70059-03-01-000	$0.93^{+0.02}_{-0.02}$	330^{+30}_{-30}	$5.21^{+0.10}_{-0.06}$	$2.3^{+0.7}_{-0.7}$	$3.56^{+0.07}_{-0.07}$	$0.155^{+0.003}_{-0.003}$	$3.04^{+0.03}_{-0.02}$	57.9/35
93408-01-23-02	$0.92^{+0.04}_{-0.03}$	270^{+30}_{-40}	$4.05^{+0.3}_{-0.13}$	$3.5^{+1.0}_{-1.0}$	$3.52^{+0.14}_{-0.13}$	$0.119^{+0.004}_{-0.004}$	$2.34^{+0.03}_{-0.06}$	40.6/36
95334-01-03-08	$0.94^{+0.02}_{-0.02}$	490^{+60}_{-60}	$8.3^{+0.2}_{-0.2}$	$4.7^{+1.5}_{-1.5}$	$3.39^{+0.09}_{-0.09}$	$0.243^{+0.006}_{-0.006}$	$4.70^{+0.11}_{-0.05}$	32.7/36
96423-01-11-01	$0.90^{+0.02}_{-0.02}$	410^{+40}_{-30}	$5.84^{+0.11}_{-0.11}$	$1.8^{+0.7}_{-0.7}$	$3.41^{+0.06}_{-0.06}$	$0.171^{+0.002}_{-0.003}$	$3.31^{+0.02}_{-0.02}$	30.9/36

emission given Table 1, and only allow the flux (i.e. model normalization) to vary. We also tested various other τ and T_e values, even allowing both of them to vary, and found that the results do not change qualitatively for the particular choice of these parameters. The results did not differ either between the different fitting methods in a qualitative sense. That is, the best fitting parameters and their evolution during the bursts were largely unaffected even if we modeled, or subtracted, the persistent emission as a background. The only difference in the second method was that during the bursts the COMPTT component could freely result in fluxes that were smaller than prior to the onsets of the bursts shown in Table 1. We decided to display the parameter evolution using the second method, but we re-iterate that the other modeling methods and slightly different choices in fixing parameters yield comparable results.

Finally, we modeled the burst spectra with only the COMPTT model, to study the possibility that occasionally the entire NS is covered beneath the spreading layer. For these fits we show only the goodness of fit measure in the subsequent figures.

3.4 Burst parameter evolution

Three example burst spectra are shown in Fig. 4 for the burst occurring during OBSID 70059-03-01-000, together with the persistent spectrum shown with black lines. The dotted lines mark the spectrum of the COMPTT component, except in the spectrum at 13.5 s from the burst onset, in which COMPTT is the only spectral component and therefore marked as a solid line. During this time, a blackbody spectrum has almost an identical shape when compared to the COMPTT model shape (the COMPTT component in the spectrum at 3.25 s overlaps almost exactly the data points of the spectrum at 13.5 s), making it difficult to constrain the parameters of the blackbody model. The addition of the COMPTT component removes the wavy residuals of the blackbody fits.

The time evolution of the spectral parameters for the XSPEC spectral fits are shown in Fig. 5 for the four highly non-Planckian bursts. The black lines show the results from the blackbody fits (grey bands indicate 1σ errors for each parameter). The blue and yellow lines (and 1σ error bands colored with lighter shades) show the results of the blackbody and COMPTT components, respectively, with the reduced χ^2

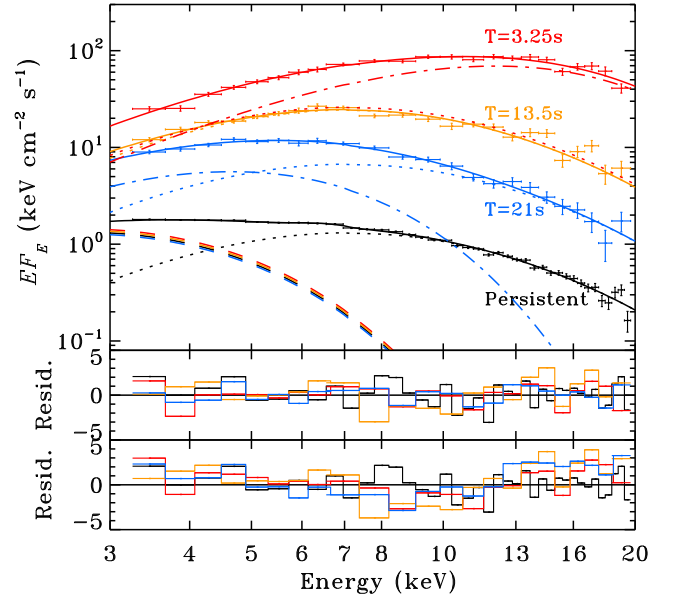


Figure 4. Example energy spectra of the burst and persistent emission from OBSID 70059-03-01-000. The solid line shows the total model spectrum, the dotted line shows the variable COMPTT component, the dashed line shows the non-variable DISKBB component, and the dot-dashed line shows the burst blackbody emission. Note that for the burst spectrum at 13.5 s from the burst onset the spectrum can be fitted only with the COMPTT component. The middle panel shows the residuals (in units of σ) from the variable COMPTT + (BB and/or DISKBB) fits. The bottom panel shows the residuals for the BB fits, which systematically underpredicts the burst emission above ≈ 13 keV.

of the fits displayed with a green line in the bottom panel. The bottom panel also shows the χ^2_{red} for the case where the entire burst spectrum is modelled only with the COMPTT model (pink lines).

The COMPTT + BB model provides a highly significant improvement to the fit for these 4 bursts with respect to the BB model fit. The fits indicate that the COMPTT component is the dominant spectral component particularly in the beginning of the cooling phase of the burst, often being consistent of carrying 100 per cent of the burst flux. It

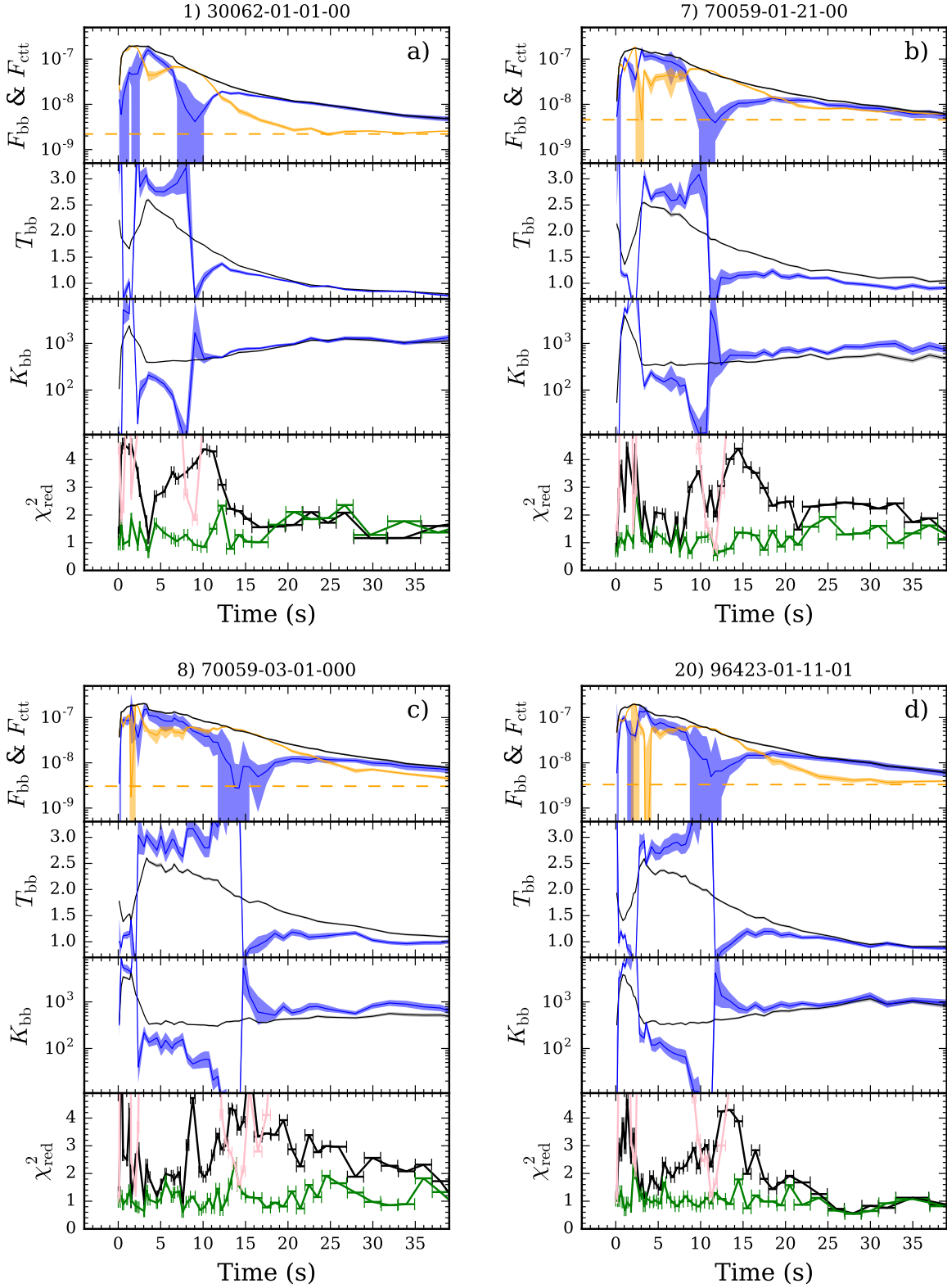


Figure 5. Time evolution of the model parameters fitted to the 4U 1608–52 PRE burst spectra during the soft spectral state. Black lines show the time evolution of the blackbody model parameters from a classic blackbody fit. Blue and orange lines show the evolution of the model parameters of the two-component model consisting of a blackbody (BB) and Comptonization (COMPTT) components, respectively. COMPTT parameters were fixed to the averaged value fitted to the spectra observed prior to the bursts, and only COMPTT normalization (i.e. flux) was left free to vary. The COMPTT flux level prior to the burst is shown with a dashed line. In the bottom panels, the green, pink and black lines show the reduced chi-squared values for the two-component, pure Comptonization (i.e. no burst blackbody component at all) and pure blackbody fits, respectively.

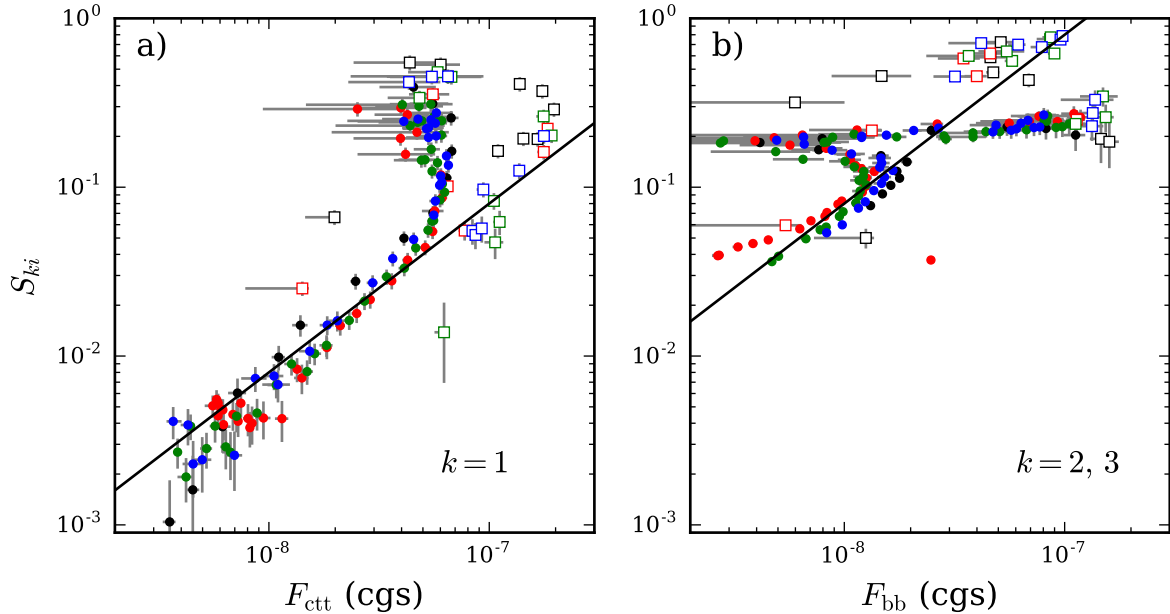


Figure 6. Comparison between the NMF signals to the fluxes obtained from the spectral fits. (a) The signal for the $k = 1$ component, S_{ki} , versus the COMP TT flux, F_{ctt} . (b) The signal for the $k = 2, 3$ component versus the BB flux, F_{bb} . The black, red, green and blue colours correspond to the four different bursts shown in Fig. 5(a), (b), (c) and (d), respectively. Squares and circles highlight spectra that occur in the PRE-phase and the cooling tail, respectively. A one-to-one relationship holds for fluxes below $F_{\text{ctt}} \lesssim 6 \times 10^{-8} \text{ erg cm}^{-2} \text{ s}^{-1}$, indicating that the direct spectral modeling works well in this range. In the end of the PRE-phase, and the early cooling tail the spectral fits and the NMF decomposition yield highly contradictory results.

is during these times that the parameters of the blackbody component become unconstrained in the XSPEC fits. This result is different with respect to the NMF decomposition, where we saw that the $k = 1$ component (corresponding to the COMP TT model) signal S_{1i} is comparable to the summed $k = 2, 3$ one. In fact, by comparing the parameter evolution to the NMF decomposition in Fig. 3 we see that the XSPEC fitting results are very different in the brightest parts of the bursts. For example the PRE phase seems to be dominated by the COMP TT component, whereas the NMF decomposition shows that the highest signal comes from the varying blackbody components ($k = 2, 3$). Here it is important to keep in mind the major difference between the two methods: Fitting spectra in XSPEC is done individually for each timestep whereas the NMF decomposition tries to minimize a global cost function spanning over the whole burst. This difference is discussed more in the Sect. 4.

While in the blackbody fits – and in the NMF decomposition – the parameter evolution is smooth, we see that in the two component fits the burst temperature shows much more rapid swings from cold to hot phases (and back) during the bursts. As we discuss below, these rapid changes are likely due to fitting degeneracies and do not correspond to real changes of the burst temperature. During these temperature swings two noticeable things occur. First, we see that the swings coincide with the times when the COMP TT-only fits provide a much better fit than the blackbody model (compare pink and black χ^2_{red} curves). Secondly, in some cases the swings occur a couple of seconds after the blackbody temperature has a clear kink in its evolution, typically about

7 seconds after the burst onsets.¹ That is, before the kink occurs the blackbody temperature falls down much more slowly than after it. It is only during this “slow cooling” stage that we can observe the constant blackbody radii in the blackbody fits, which are not predicted by the atmosphere models (Suleimanov et al. 2012).

To highlight the differences between the two decompositions, we compare the strength of the $k = 1$ NMF signals, S_{ki} , and the COMP TT component fluxes, F_{ctt} , in Fig. 6(a). Similarly, in Fig. 6(b), we compare the $k = 2, 3$ NMF signals to the blackbody component fluxes, F_{bb} . There is a clear one-to-one relationship for fluxes below $F_{\text{ctt}} \lesssim 6 \times 10^{-8} \text{ erg cm}^{-2} \text{ s}^{-1}$ for all four bursts (highlighted with different colours). Also, during the PRE-phase of these bursts that lasts between 3.25–3.5 s (shown by squares), the spectra show roughly similar F_{ctt} as compared to the $F_{\text{ctt}} - S_{ki}$ trend line later in the cooling tail. Similar behavior is also seen in Fig. 6(b). However, the differences are highly notable in the end of the PRE-phase and in the early cooling stage where according to the COMP TT + BB fits the COMP TT component dominates. The model fits simply do not agree with the NMF decomposition results in this range, which probably arises from the spectral degeneracy of the COMP TT and blackbody components.

The results from the other four PRE-bursts in the soft state show similar behavior, albeit the presence of the second spectral component is less clear as can be seen in Fig. 7. The model parameter evolution in the panels Fig. 7(a)–(d) show that the burst spectra is fitted adequately (except the first

¹ In some decompositions with different COMP TT parameters these two times coincide.

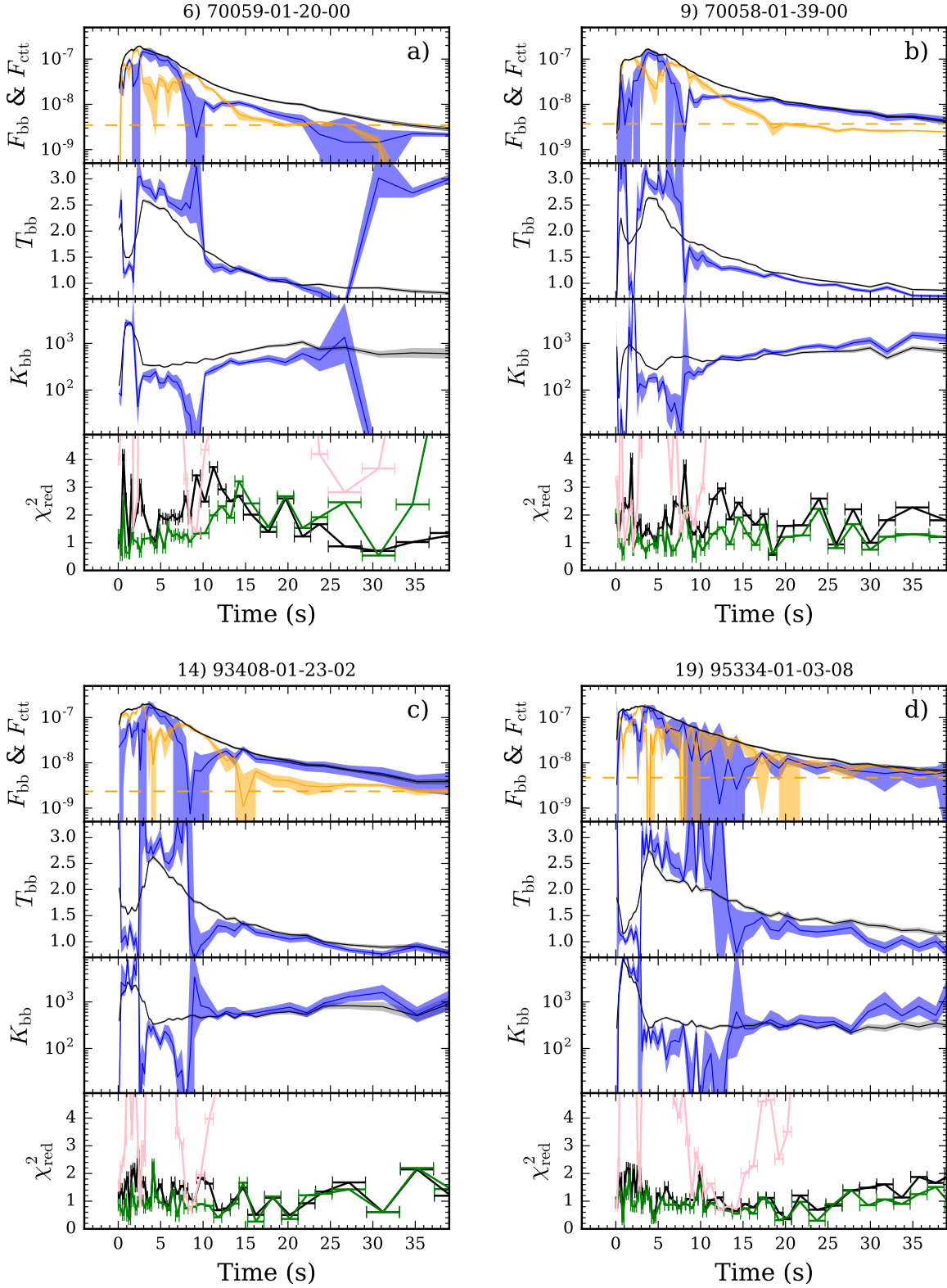


Figure 7. Same as Fig. 5, but for four other soft-state PRE bursts.

10–15 s) with a pure blackbody model and, consequently, the COMPTT component becomes less constrained and unnecessary. It is worth highlighting, however, that very similar trends can be observed as compared to the bursts in Fig. 5, thus the same physical processes are likely to take place.

We also performed similar analysis for the hard state bursts. In Fig. 8, we show the time evolution of the model parameters taken from four bursts that were used by Poutanen et al. (2014) to derive the NS mass, radius and distance of 4U 1608–52. These fits show clearly that in the PRE phase and during the early cooling phases the blackbody model fits the data well. Only at lower fluxes we see values of $\chi^2_{\text{red}} \approx 2$, and more importantly the fits are not improved by adding the COMPTT model. This difference is further highlighted in Fig. 9, where we show the χ^2_{red} distributions for the soft (left panel) and hard state bursts (right panel). We can see that for the soft state bursts the addition of the COMPTT component brings the observed distribution close to the expected one, whereas in the hard state the bad fits during the end of the cooling tails are not removed.

4 DISCUSSION

The non-Planckian spectra seen during the soft state PRE-bursts of 4U 1608–52 are caused by another spectral component that is well described by an optically thick Comptonized emission that we model using COMPTT.² The results indicate clearly that the parameters of the COMPTT component during the X-ray bursts share many similarities with the parameters of the spreading layer that forms in the accretion disc-NS boundary, both from theoretical perspective (Inogamov & Sunyaev 1999, 2010; Suleimanov & Poutanen 2006), with respect to previous observations of the persistent emission (Gilfanov et al. 2003; Revnivtsev & Gilfanov 2006; Revnivtsev et al. 2013), as well as the 4U 1636–536 superburst data (Koljonen et al. 2016). The spreading layer model essentially suggests that the layer – that spreads from the NS equator (disc mid-plane) towards the NS rotational poles – is levitating above the NS surface, and the bulk of the emission is released in two bands located above the equator and up to a latitude higher up that is determined by the mass accretion rate. Each latitude in these emission bands emit quasi-thermal emission at its local Eddington limit (Suleimanov & Poutanen 2006). The model predicts a roughly constant (Eddington) temperature emission from each latitude, and that the latitudinal width is solely determined by the emitted flux, which is proportional to mass accretion rate. Given that the spreading layer spectral shape is constant irrespective of the emitted flux, the model thus naturally explains why during the soft state (i.e. banana branch) the hard X-ray colour of 4U 1608–52 (and other “atoll” sources) remains constant over a large range of observed fluxes (Gilfanov et al. 2003; Revnivtsev & Gilfanov 2006; Revnivtsev et al. 2013).

The spreading layer carries a little less than 40 per cent of the persistent flux in the cases we studied, consistent with the findings of Takahashi et al. (2011) who analyzed the

persistent emission of 4U 1608–52 using *RXTE* data. However, as can be seen in Fig. 4, the spreading layer actually dominates the persistent emission in the 3–20 keV spectral band of the PCA instrument, particularly above ~ 7 keV. Therefore, the method of multiplying the entire persistent spectrum with a constant (Worpel et al. 2013, 2015) – which was found to be spectral state dependent in 4U 1608–52 (Ji et al. 2014) – is indeed very similar to our approach. On the other hand, our interpretation of the whole phenomenon is very different. Similarly to the superburst of 4U 1636–536 (Koljonen et al. 2016), the non-parametric NMF decomposition clearly shows that only the spreading layer component is variable during the bursts and the disc component that dominates at lower energies remains constant. As the disc likely extends down to the innermost stable circular orbit (or the NS surface), it should get hotter if the prevailing mechanism for the persistent emission change is an increase of the mass accretion rate through the Poynting-Robertson drag mechanism, as suggested by Worpel et al. (2013, 2015). This heating and the subsequent cooling of the disc during the burst tail, is not seen in the NMF analysis nor is it needed to describe the spectral changes.

An alternative interpretation was proposed by Koljonen et al. (2016) based on the 4U 1636–536 superburst data. The observed variations of the COMPTT component can be interpreted as changes in the latitudinal width of the spreading layer in the course of the X-ray burst. The layer is proposed to be levitating above the NS surface, because it is being pushed outwards by the radiation pressure approaching the Eddington limit (Inogamov & Sunyaev 1999, 2010; Suleimanov & Poutanen 2006). Clearly, during the X-ray burst, the increased emission from the burst must travel through this layer near the NS equator providing additional pressure support. We propose that – as a consequence of the increased emission – the layer is being pushed towards higher latitudes, perhaps completely engulfing the NS as the burst emission approaches the Eddington limit. Hence, rather than seeing a bursting NS atmosphere near the burst peak, we see a large fraction of the burst emission passing through the spreading layer, and subsequently, as the burst flux decays the spreading layer latitudinal width decreases, ultimately returning to its original state observed prior to the X-ray burst.

Such phenomenon was speculated to exist by Suleimanov et al. (2011b) – and also by Poutanen et al. (2014) and Kajava et al. (2014) – to describe why the blackbody radii immediately after the photospheric touchdown were constant in soft state bursts. The blackbody radii of the undisturbed NS atmosphere are not expected to be constant, given that they depend on the colour correction factor as $R_{\text{bb}} \propto f_c^{-2}$, as f_c has a strong dependency on the emitted flux, especially near the Eddington limit (Suleimanov et al. 2011a, 2012). The models predict a very characteristic increase of the blackbody radii in the beginning of the cooling stage, almost identical to what is seen in the hard state bursts of 4U 1608–52 (see Fig. 8 and Poutanen et al. 2014). Soft state bursts of 4U 1608–52 do not show this behavior, nor do any other NS-LMXBs in the soft state (Kajava et al. 2014). Our results indicate that the constant blackbody radii in the blackbody analysis may be caused by the spreading layer; the only way to obtain this is by having a constant colour correction factor as a function of flux, which

² Note that non-Planckian spectra from 4U 1608–52 have been observed also with TENMA (Nakamura et al. 1989).

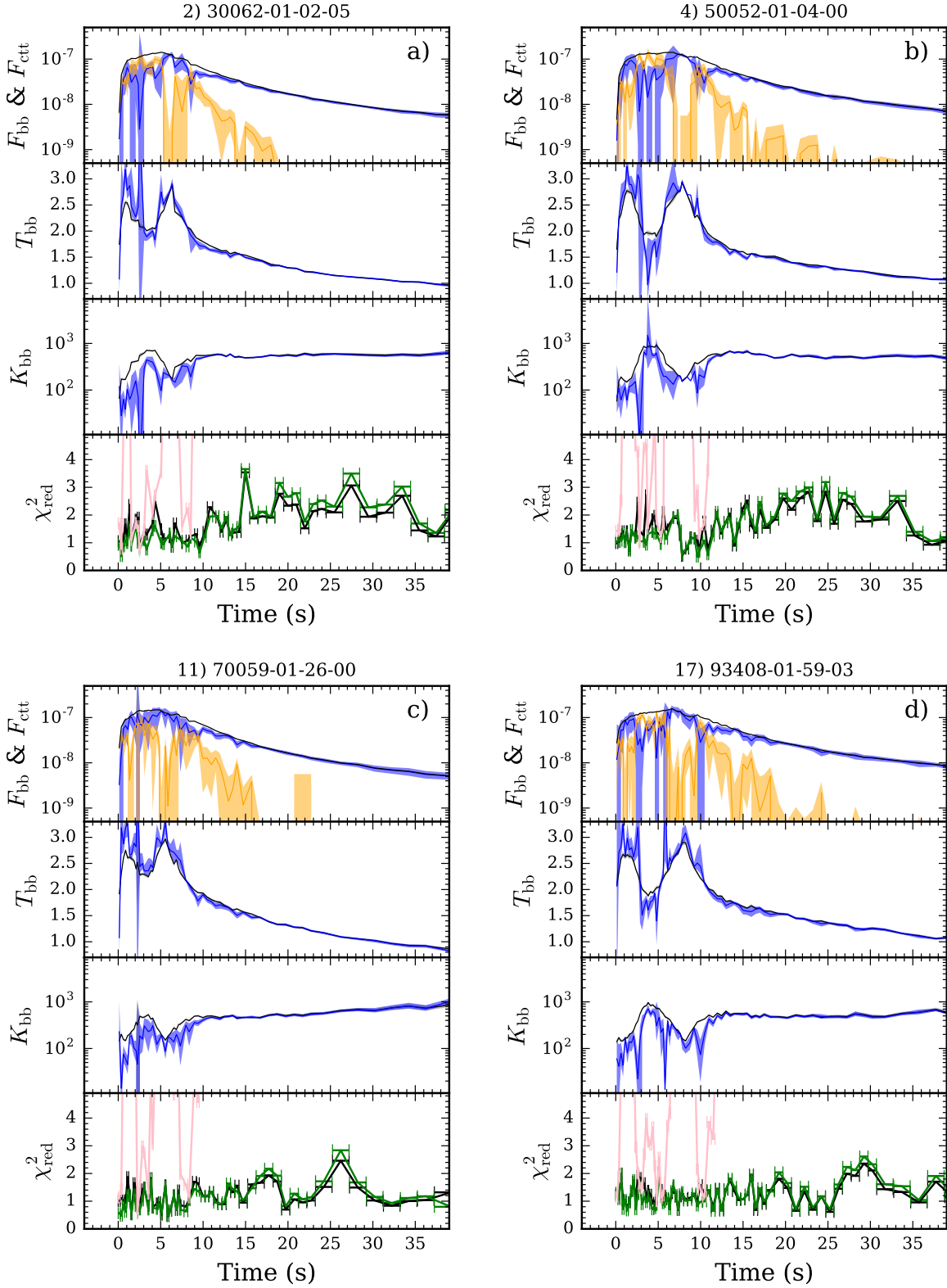


Figure 8. Same as Fig. 5, but for four hard-state PRE-bursts that were used by Poutanen et al. (2014) to determine the NS mass and radius of 4U 1608–52. Note that the pre-burst spectrum has been subtracted as a background. The burst spectra are well fitted with a blackbody model, and adding the COMPTT component does not improve the fits, not even in some burst tails where the blackbody fits resulted in $\chi_{\text{red}}^2 \approx 2$.

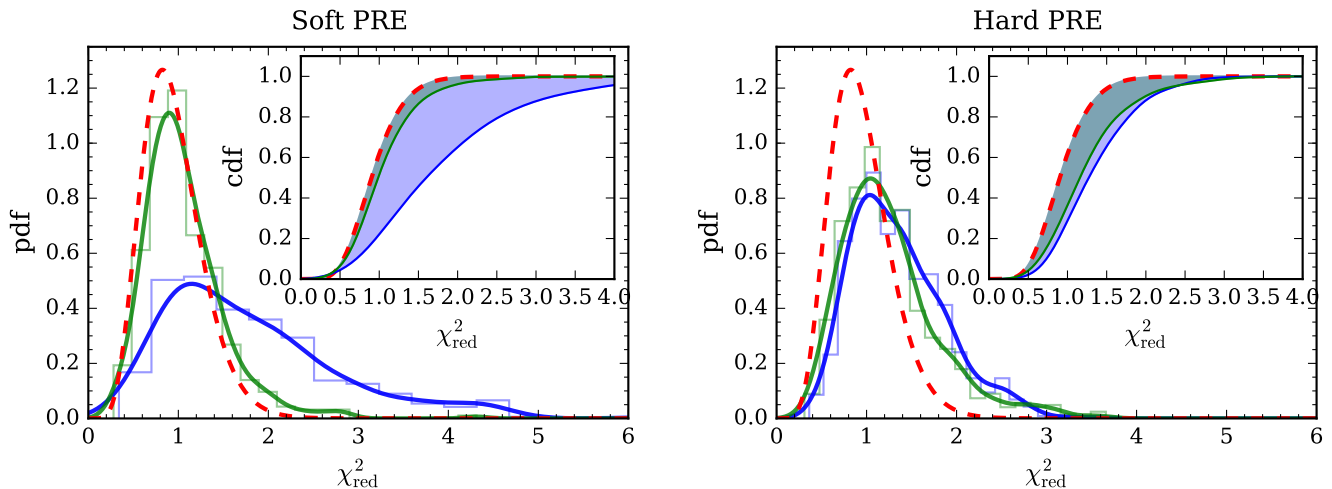


Figure 9. Reduced χ^2 distributions for the soft-state (left panel) and the hard-state (right panel) PRE burst spectra. The step-line shows the underlying histogram of the distribution while the thick solid lines correspond to Gaussian kernel density estimates of the distribution. Green and blue lines show the estimates for the BBODYRAD+COMPTT and BBODYRAD models, respectively. Red dashed lines show the expected theoretical distributions (for d.o.f. equal to 17, a typical value for the observed spectral bins). Insets in the upper right corners show the cumulative distributions where the deviations from the theoretical distribution are highlighted with green and blue shadings. All the distributions are normalized so that the area encapsulated by the curve is unity.

is predicted by the spreading layer model (Suleimanov & Poutanen 2006).

The results provide important insights with respect to the NS mass and radius determination using PRE-bursts. If the NS surface is partially covered by the spreading layer a number of assumptions mentioned in the introduction are not valid. Firstly, we do not see the whole undisturbed NS surface, but rather a part of the atmosphere is covered by the spreading layer, through which the burst emission has to penetrate. Secondly, a part (the lower half) of the NS surface is blocked by the optically thick accretion disc that is connected to the spreading layer. Thirdly, the spreading layer has a colour correction factor that is in the range of $f_c \sim 1.6$ – 1.8 irrespective of the flux. When the soft-state bursts are used to determine the blackbody radii from the touchdown flux down to a small fraction of it (Güver et al. 2010; Özel et al. 2016), the radii are mapped into the NS radius and mass space by implicitly assuming that the touchdown flux is the Eddington flux, that the NS is entirely visible and that the colour correction factor lies in between $f_c = 1.3$ – 1.4 . The latter two are clearly not correct assumptions, and probably not the first one either. Note that the bursts shown in Fig. 5(a,c) were used by Güver et al. (2010) to determine the Eddington flux F_{Edd} (more recently Özel et al. 2016 also added the burst shown in Fig. 7d). In these bursts, and in all bursts shown in Figs 5 and 7 in general, one can see that the spreading layer component reprocesses roughly the half of the emitted burst flux.

There are still some uncertainties in the analysis that remain open. For example, the “bottom half” of the NS should be covered by the accretion disc, but the touchdown fluxes are higher in the soft state compared to the hard state. At first glance this observational fact could be considered to be inconsistent with our interpretation of the data. However, the reflection of the burst emission off the inner accretion disc (Lapidus & Sunyaev 1985) could cause stronger

anisotropy of the emission in the soft state, where the inner disc edge is likely closer to the NS than in the hard state. Thus, the burst emission could be boosted more in the soft-state bursts, as was argued by Suleimanov et al. (2016). However, in this case reflection features should be detected in the form of iron emission lines and photo-ionization edges. Unlike in the superburst data where these features are clearly seen (Strohmayer & Brown 2002; Ballantyne & Strohmayer 2004; Keek et al. 2014; Koljonen et al. 2016), the 4U 1608–52 soft state burst spectra do not require them. Furthermore, when the burst emission irradiates the inner disc, a fraction of it may be absorbed rather than reflected enhancing the disc flux. This effect does not seem to be present either. As mentioned above, such disc heating should manifest as another NMF component, which is not detected in the analysis. It is possible that we are not detecting these features in 4U 1608–52 simply because of the limited sensitivity compared to the superburst data, and thus future observations with *Astrosat*, *NICER* and/or *eXTP* may help to address this issue.

Another curious feature is related to the size scales during the first three seconds of the radius expansion phase, during which the COMPTT component carries a large fraction of the emitted flux. From the black body component we can estimate that black body radii are roughly 3 times larger during the PRE than in the burst tail. This indicates that the photospheric radius expansion is few tens of kilometers (note that here the unknown color correction factor in the PRE phase plays a critical role; see Poutanen et al. 2014; Kajava et al. 2017a). On the other hand, according to Inogamov & Sunyaev (2010) the radial width of the spreading layer is only a few hundred meters, and thus the layer (and the inner accretion disc) should be hidden underneath the expanded burst atmosphere. The data clearly indicates that the spreading layer is visible, and it is not clear how this is possible. We can only speculate that the radius expansion

is not symmetric for some reason, such that the expansion occurs predominately in the NS poles.

Another unclear issue is that there are some bursts where the spreading layer returns to its original state within 15 s (e.g. bursts in Fig. 5a and Fig. 7a), whereas in others the spreading layer is active longer. Also, some bursts are clearly much more non-Planckian than others and there does not appear to be any common factor behind these differences in terms of the burst onset conditions, i.e. the persistent emission level or the X-ray colours. The biggest issue, however, is clearly the difficulty to disentangle the two spectral components when the burst blackbody temperature is in the range of $T_{\text{bb}} \sim 2.0\text{--}2.4$ keV. Whenever the temperature passes through this range we see violent jumps from cold to hot phases in the model parameters during the PRE stage, and vice versa in the cooling tail. The fact that such rapid changes – and the corresponding BB component flux swings – are not seen in the NMF decomposition means that they are without a doubt just modeling artifacts. These discrepancies are likely related to the fitting differences. In the XSPEC fitting, the COMPTT component is not allowed to vary in shape but only in normalization, whereas the blackbody can have any temperature or normalization. Because in the $T_{\text{bb}} \sim 2.0\text{--}2.4$ keV range the blackbody and the COMPTT produce very similar spectral shapes, the COMPTT remains a stable component as only its flux is allowed to vary, and the two blackbody parameters then act to compensate the small residuals left in the data. In contrast in the NMF analysis all the burst spectra are decomposed into three linear components that all have fixed “shapes”, and therefore these components do not compete in the cost function minimization when the summed spectral shape of the $k = 2, 3$ components corresponds to the $k = 1$ shape.

Therefore, the most likely scenario is that a small polar cap is always directly visible, with the rest of the NS being covered underneath the spreading layer at touchdown. Once the flux starts decaying and the atmosphere cools, the NS also becomes gradually more visible. We speculate that – as the NS is oblate given its large spin frequency of ≈ 620 Hz (Watts 2012) – the pole should have larger gravitational pull than the equatorial regions, and thus the burst blackbody can attain higher Eddington temperatures at the poles compared to the regions covered by the spreading layer. However, we cannot completely rule out a possibility that the entire NS is covered by the spreading layer until the point in time when the temperature jump occurs, and the hottest parts of the bursts may just be caused by the spreading layer spectrum changing its temperature when the entire NS becomes covered. For example, in the burst shown in Fig. 7(d) the cooling seems to stall for up to five seconds, during which the spectrum is identical to the spreading layer. This similarity favours the latter interpretation, but the fact that the peak temperatures are $T_{\text{bb}} \sim 3.0$ keV, just like in the hard-state bursts, lends support to the former scenario. From the 4U 1608–52 data alone it is not clear which one actually happens and a more systematic comparison between various bursters is warranted in the future. It is also not clear how scalable these results are with respect to other bursters. While some sources show similar non-Planckian spectra as 4U 1608–52 in the soft state and correspondingly constant blackbody radii in the initial cooling tail (Güver et al. 2012), other sources do not. Here, however, it is important to study

the bursts as a function of spectral state (as in Zhang et al. 2011), as in the hard state other effects than the spreading layer may also distort the persistent spectra, for example, the burst-induced cooling of the coronae (Ji et al. 2015; Degenaar et al. 2016; Kajava et al. 2017b), or by the intermittent presence of metals in the NS photospheres (Nättälä et al. 2015; Kajava et al. 2017a).

5 SUMMARY

In this paper we have presented a study of X-ray bursts from the LMXB 4U 1608–52, mainly focusing on the PRE bursts that occur while the system is in the soft spectral state. Using the non-parametric NMF spectral decomposition method, we found that during most of the non-Planckian PRE bursts in the soft state there are in fact two variable spectral components during the bursts. One component is well described with a variable temperature X-ray burst black body component, while the other component is identical to the spreading layer that forms in the interface between the accretion disc and the NS surface. We find that during the bursts the spreading layer component brightens by a factor up to about 50. This occurs, in our view, because the enhanced radiation pressure provided by the X-ray burst emission underneath the spreading layer pushes it towards the NS poles, possibly engulfing the entire NS surface during the brightest phases of the bursts.

This physical picture provides an alternative interpretation to the apparent increase of the persistent emission level during the bursts through the Poynting-Robertson drag mechanism, as proposed by Worpel et al. (2013, 2015). Instead, we argue that the burst emission is reprocessed in the spreading layer as it passes through it, causing the layer to have a variable latitudinal width in the course of the bursts, which only mimics an increase of the persistent emission.

Due to this interplay, the burst emission gets distorted and thus the spectral color correction factor, that is used in determining NS masses and radii is much higher than for a passively cooling NS atmosphere. Furthermore, as the layer is optically thick, a fraction of the NS that would be visible due to light bending effects is hidden in these soft state bursts. These two factors together are the likely causes for the significantly different NS mass and radius constraints obtained using the soft state bursts vs. the hard state bursts, where the spreading layer does not play a role in shaping the burst spectra.

ACKNOWLEDGEMENTS

We thank the anonymous referee for helpful suggestions that improved the manuscript. JJEK was supported by Academy of Finland grants 268740 and 295114. JN was supported by the University of Turku Graduate School in Physical and Chemical Sciences. VFS was supported by the German Research Foundation (DFG) grant WE 1312/48-1 and by the Russian Government Program of Competitive Growth of Kazan Federal University. JP thanks the Foundations’ Professor Pool, the Finnish Cultural Foundation and the National Science Foundation grant PHY-1125915 for support.

REFERENCES

- Arnaud K. A., 1996, in Jacoby G. H., Barnes J., eds, *Astronomical Society of the Pacific Conf. Ser. Vol. 101, ADASS V*. p. 17
- Ballantyne D. R., Strohmayer T. E., 2004, *ApJ*, **602**, L105
- Bildsten L., Salpeter E. E., Wasserman I., 1992, *ApJ*, **384**, 143
- Burke M. J., Gilfanov M., Sunyaev R., 2017, *MNRAS*, **466**, 194
- Degenaar N., Koljonen K. I. I., Chakrabarty D., Kara E., Altamirano D., Miller J. M., Fabian A. C., 2016, *MNRAS*, **456**, 4256
- Done C., Gierliński M., Kubota A., 2007, *A&ARv*, **15**, 1
- Gierliński M., Done C., 2002, *MNRAS*, **337**, 1373
- Gilfanov M., Revnivtsev M., Molkov S., 2003, *A&A*, **410**, 217
- Güver T., Özel F., Cabrera-Lavers A., Wroblewski P., 2010, *ApJ*, **712**, 964
- Güver T., Özel F., Psaltis D., 2012, *ApJ*, **747**, 77
- Hoffman J. A., Cominsky L., Lewin W. H. G., 1980, *ApJ*, **240**, L27
- Inogamov N. A., Sunyaev R. A., 1999, *Astronomy Letters*, **25**, 269
- Inogamov N. A., Sunyaev R. A., 2010, *Astronomy Letters*, **36**, 848
- Jahoda K., Markwardt C. B., Radeva Y., Rots A. H., Stark M. J., Swank J. H., Strohmayer T. E., Zhang W., 2006, *ApJS*, **163**, 401
- Ji L., Zhang S., Chen Y., Zhang S.-N., Torres D. F., Kretschmar P., Li J., 2014, *ApJ*, **791**, L39
- Ji L., et al., 2015, *ApJ*, **806**, 89
- Kajava J. J. E., et al., 2014, *MNRAS*, **445**, 4218
- Kajava J. J. E., Nättälä J., Poutanen J., Cumming A., Suleimanov V., Kuulkers E., 2017a, *MNRAS*, **464**, L6
- Kajava J. J. E., Sánchez-Fernández C., Kuulkers E., Poutanen J., 2017b, *A&A*, **599**, A89
- Keek L., in’t Zand J. J. M., Kuulkers E., Cumming A., Brown E. F., Suzuki M., 2008, *A&A*, **479**, 177
- Keek L., Ballantyne D. R., Kuulkers E., Strohmayer T. E., 2014, *ApJ*, **797**, L23
- Koljonen K. I. I., 2015, *MNRAS*, **447**, 2981
- Koljonen K. I. I., Kajava J. J. E., Kuulkers E., 2016, *ApJ*, **829**, 91
- Lapidus I. I., Sunyaev R. A., 1985, *MNRAS*, **217**, 291
- Lattimer J. M., 2012, *Annual Review of Nuclear and Particle Science*, **62**, 485
- Lewin W. H. G., van Paradijs J., Taam R. E., 1993, *Space Sci. Rev.*, **62**, 223
- Muñoz-Darias T., Fender R. P., Motta S. E., Belloni T. M., 2014, *MNRAS*, **443**, 3270
- Nakamura N., Dotani T., Inoue H., Mitsuda K., Tanaka Y., Matsuoka M., 1989, *PASJ*, **41**, 617
- Nättälä J., Suleimanov V. F., Kajava J. J. E., Poutanen J., 2015, *A&A*, **581**, A83
- Nättälä J., Steiner A. W., Kajava J. J. E., Suleimanov V. F., Poutanen J., 2016, *A&A*, **591**, A25
- Özel F., Psaltis D., Güver T., Baym G., Heinke C., Guillot S., 2016, *ApJ*, **820**, 28
- Paczyński B., 1983, *ApJ*, **267**, 315
- Poutanen J., Nättälä J., Kajava J. J. E., Latvala O.-M., Galloway D. K., Kuulkers E., Suleimanov V. F., 2014, *MNRAS*, **442**, 3777
- Revnivtsev M. G., Gilfanov M. R., 2006, *A&A*, **453**, 253
- Revnivtsev M. G., Suleimanov V. F., Poutanen J., 2013, *MNRAS*, **434**, 2355
- Strohmayer T. E., Brown E. F., 2002, *ApJ*, **566**, 1045
- Suleimanov V., Poutanen J., 2006, *MNRAS*, **369**, 2036
- Suleimanov V., Poutanen J., Werner K., 2011a, *A&A*, **527**, A139
- Suleimanov V., Poutanen J., Revnivtsev M., Werner K., 2011b, *ApJ*, **742**, 122
- Suleimanov V., Poutanen J., Werner K., 2012, *A&A*, **545**, A120
- Suleimanov V. F., Poutanen J., Klochkov D., Werner K., 2016, *European Physical Journal A*, **52**, 20
- Suleimanov V. F., Poutanen J., Nättälä J., Kajava J. J. E., Revnivtsev M. G., Werner K., 2017, *MNRAS*, **466**, 906
- Swank J. H., Becker R. H., Boldt E. A., Holt S. S., Pravdo S. H., Serlemitsos P. J., 1977, *ApJ*, **212**, L73
- Takahashi H., Sakurai S., Makishima K., 2011, *ApJ*, **738**, 62
- Watts A. L., 2012, *ARA&A*, **50**, 609
- Wilms J., Allen A., McCray R., 2000, *ApJ*, **542**, 914
- Worpel H., Galloway D. K., Price D. J., 2013, *ApJ*, **772**, 94
- Worpel H., Galloway D. K., Price D. J., 2015, *ApJ*, **801**, 60
- Zhang G., Méndez M., Altamirano D., 2011, *MNRAS*, **413**, 1913
- in’t Zand J. J. M., Weinberg N. N., 2010, *A&A*, **520**, A81

This paper has been typeset from a $\text{\TeX}/\text{\LaTeX}$ file prepared by the author.